

Dynamical Coupling of a Battery Electro-Thermal Model and the Traction Model of an EV for Driving Range Simulation

R. German, S. Shili, A. Desreux, A. Sari, P. Venet, A. Bouscayrol

Abstract— The driving range of electric vehicles is a complex issue. In simulation, this range is determined by coupling a battery model and a traction model of the vehicle. But most of the battery models used for such studies do not take into account the interaction between the temperature of the battery (impacting its electrical parameters) and the traction model of a studied EV. In this paper, a battery electro-thermal model (with all electrical parameters dependent upon the temperature) is dynamically coupled with the traction model of an electric vehicle. Simulation results are provided to show the impact of the temperature on the driving range. The initial battery model (without temperature dependence) leads to an overestimation of the driving range of 3.3% at -5°C and an underestimation of 2.5% at 40°C.

Index Terms— Electric Vehicle; System Modelling; Li-ion Battery; Characterization; Electro-Thermal Modelling.

I. INTRODUCTION

Electric vehicles (EVs) are a solution for managing petroleum depletion and reducing global carbon emissions. Nevertheless, charging time and driving range are frequent worries for future EV owners [2].

Characterization studies have shown that a cold temperature has a strong impact on the electrochemical energy storage in a battery [3]-[5]. Battery capacity fades and internal resistance increases at low temperature. In addition, the temperature affects the aging of the battery [6], [7].

As a consequence, many studies focus on the thermal behaviour of batteries for use in electric vehicles.

Some prior works use battery electro-thermal models with constant electrical parameters (no coupling between the temperature and the battery electrical parameters) [8][9].

Other researches have been focused on the characterization of electrical parameters at different temperature, but do not attempt coupling with a traction chain [10]-[13]. An interesting approach has recently been developed for battery modelling in cold weather [10].

Submitted 24 June 2019, revised 9 October 2019, accepted 15 November 2019.

Copyright (c) 2019 IEEE. Personal use of this material is permitted. However, permission to use this material for any other purposes must be obtained from the IEEE by sending a request to pubs-permissions@ieee.org.

R. German, A. Desreux and A. Bouscayrol are with Univ. Lille, Centrale Lille, Arts et Métiers Paris Tech, HEI, EA 2697 – L2EP - Laboratoire d'Electrotechnique et d'Electronique de Puissance, F-59000 Lille, France and the French network on HEVS and EVS, MEGEVH, France (email: ronan.german@univ-lille.fr, anatole.desreux@univ-lille.fr, alain.bouscayrol@univ-lille.fr)

S. Shili, A. Sari and P. Venet are with Univ Lyon, Université Claude Bernard Lyon 1, Ecole Centrale de Lyon, INSA Lyon, CNRS, Ampère, F-69100 Villeurbanne, France (email: seima.shili@univ-lyon1.fr, ali.sari@univ-lyon1.fr, pascal.venet@univ-lyon1.fr).

Table 1 Parameters and symbols

	Parameter	Name	Value	Unit
Cell	Cell capacity	C_{AhCell}	>160	A.h
	Cell nominal voltage	$U_{CellNom}$	3.3	V
	Maximal cell discharge current	I_{Cell}	480	A
	Cell interconnection resistance	R_{Con}	505	$\mu\Omega$
	Cell weight	---	5.6	kg
	Cell thermal resistance	R_{ThCell}	2.63	K/W
	Cell thermal capacitance	C_{ThCell}	2430	J/K
Battery	Battery config. (series x parallel)	$n_{SCells} \times n_{PCells}$	24 x 1	cells
	Battery nominal voltage	U_{BatNom}	79.2	V
	Battery nominal power	P_{Bat}	38.0	kW
	Battery mass	m_{Bat}	134	kg
EV traction	Aerodynamic drag coefficient	C_X	0.35	---
	Front surface	S	1.55	m ²
	Air volumic mass	ρ_{Eq}	1.3	kg/m ³
	Road friction	f_0	150	N
	Wheel radius	r_{Wheel}	0.26	m
	Reduction coefficient	k_{Red}	5.84	---
	Mechanical efficiency	η_{Mech}	0.85	---
	Electric drive peak power	$P_{DriveMax}$	25	kW
	Electric drive efficiency	η_{Drive}	[1]	---

In that work, a battery electro-thermal model has been developed based on multi-temperature characterizations of electrical parameters.

Other works couple the traction model of the vehicle with an electric model of the battery that is partly temperature dependent. For example, in [14], the OCV and SOC are directly dependent on the temperature, whereas impedance parameters are not.

The novelty of this paper is to propose a dynamical electro-thermal model (full SOC and temperature dependence for all the electrical parameters of the battery) in dynamical interaction with the traction model of the vehicle.

First, a thermal model is dynamically coupled with the electrical part of the battery model. This coupling leads to temperature dependence on the electrical parameters and electrical parameters dependent on the temperature. Thus, for a specified battery current, the battery voltage is affected by the temperature evolution. Second, this electro-thermal dynamical battery model is coupled to a dynamical model of the traction subsystem of the EV. The traction current is then updated from the battery voltage evolution, which is itself affected by the battery temperature evolution.

The battery model is organized using EMR (Energetic Macroscopic Representation) [15] to provide easy interconnection with a complete traction model. EMR is a graphical formalism to organize models and control of multiphysical energy conversion systems. It has been used in

the field of electric and hybrid vehicles for its ability to develop control structures in a systematic way although other formalisms also exist for vehicle model organization [16]. A first paper has already proposed an electro-thermal model of a battery using EMR [17], but with fixed electrical parameters (characterized at 25 °C). This new model is temperature dependent. Thus, it enables the study of driving range at several temperatures.

This paper is limited to the impact of the battery temperature on the driving range. Ancillary systems supplied by the battery are known to significantly increase the battery current (i.e., heating [18] [19] and air conditioning [20][21]). They are not considered in this paper.

In section II the coupled electro-thermal battery model is organized using EMR and then linked with the traction subsystem model. In section III, a cell from an actual EV is characterized at several temperatures. In section IV, the battery model is validated at the system level with on-board measurements in the vehicle. In section V, the impact of the temperature on the driving range is studied by simulation.

II. CAUSAL ORGANIZATION OF THE EV MODEL

A. Electro-thermal model for one cell

The electric model (Fig. 1) is a classical equivalent circuit model composed of 3 parts [4]:

- The Open Circuit Voltage (OCV_{Cell}) is linked to the energy stored by electrochemical mechanisms (OCV_{Cell} increases with the state of charge SoC).
- The series resistance (R_{SCell}) represents the sum of the conduction, the ionic transport in electrolyte and the charge transfer resistances. The double-layer capacitance is neglected given the time constants considered (greater than few seconds).
- The phenomena related to the insertion and diffusion of the ions in the battery nanostructure is represented by a $R_{DiffCell}/C_{DiffCell}$ parallel equivalent circuit instead of a Warburg impedance as in [22]. This model is a compromise between accuracy and computation time for embedded systems [10].

The chosen electrical model (Fig. 1) includes full SOC and temperature dependence of all the electrical parameters, unlike prior related work [17].

The Peukert effect (i.e. the dependence of the battery recoverable capacity with discharge current) can be neglected for the LFP battery technology (Peukert constant between 0.99 and 1.04) [23]. LFP stability with current rate is confirmed by previous works [24].

The thermal model of the battery (Fig. 2) is a standard averaged thermal model built with the following hypothesis [25]:

- The thermal capacitance of the cell core (the inside part of the cell) C_{ThCell} is taken into account. The thermal capacitance of the cell surface is neglected as its package is very lightweight compared to the core.
- The equivalent thermal resistance r_{ThCell} represents the heat transfer between the core to the surface (conduction) and the surface to the air (convection).

The heat power (P_{Heat}) is assumed to come only from the joule effect in R_{SCell} and $R_{DiffCell}$ (1).

$$P_{Heat} = R_{SCell} \cdot i_{Cell}^2 + R_{DiffCell} \cdot i_{RDiffCell}^2 \quad (1)$$

As in [10], the electrical and thermal part of the model are coupled by the internal temperature and the heat power (Fig. 3).

B. EMR of the cell electro-thermal model

In order to highlight the coupling of the electrical and thermal parts of the cell model, the EMR (Energetic Macroscopic Representation) formalism is used. It will later enable an easy coupling of the battery model with the traction subsystem model.

EMR [15] is a functional and graphical description using pictograms (see Annex A). EMR highlights the power exchange between different multi-domain elements by the action-reaction variables. In that way, the product of the action and reaction variables leads to the instantaneous power. Moreover, EMR is based on the causality principle. With causality, the output can only be an integral function of the inputs (see Fig. 4), i.e. the output can only be a consequence of the inputs, obtained after a delay from the input changes.

In [10], the electro-thermal model is not organized according to the causality principle. In order to better understand the interaction between the thermal and electrical parts, this model is reorganized in a causal way using EMR (Fig. 5). This new organization will enable an easy coupling with the traction subsystem model later.

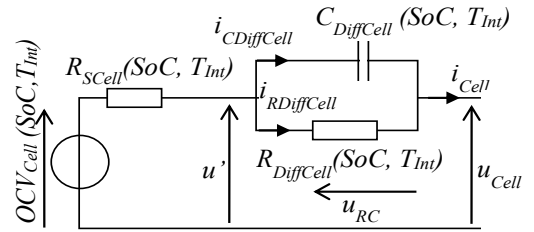


Fig. 1 Structure of the electric model for one cell

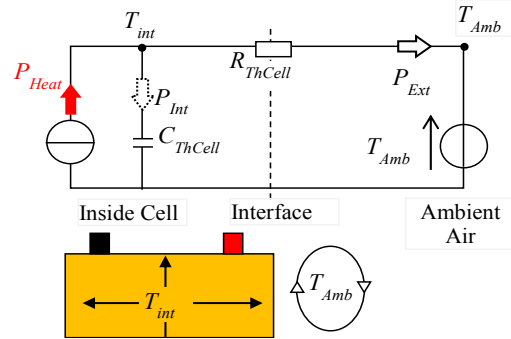


Fig. 2 Structure of the thermal model for one cell [17]

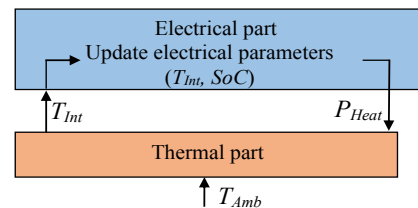


Fig. 3 Electro-thermal coupling principle

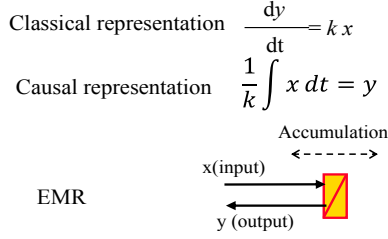


Fig. 4 From classical representation to EMR

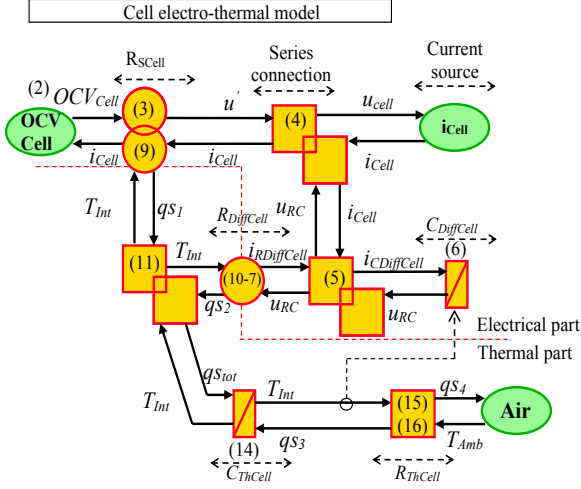


Fig. 5 EMR of the dynamical electro-thermal model [17]

The SoC is calculated from the integration of the current, the initial SoC and the discharge capacity of the cell (2).

$$SoC(\%) = SoC_{Init} - \frac{100}{3600 \cdot C_{AhCell}} \int_0^{t_{Ch/Dch}} i_{Cell} dt \quad (2)$$

OCV_{Cell} is represented as a source of voltage in EMR (green oval). The resistance R_{SCell} is represented as a conversion element as there is no delay (integral) between inputs and outputs (3).

$$OCV_{Cell} - R_{SCell} \cdot i_{Cell} = u' \quad (3)$$

The series connection is a coupling element i.e. a distribution of energy (4).

$$u' - u_{RC} = u_{Cell} \quad (4)$$

The parallel connection (current node) is also a coupling element (5).

$$i_{Cell} - i_{RDiffCell} = i_{CDiffCell} \quad (5)$$

$C_{DiffCell}$ is an accumulation element i.e. storage of energy (6).

$$u_{RC} = \frac{1}{C_{DiffCell}} \int_0^t i_{CDiffCell} dt \quad (6)$$

$R_{DiffCell}$ is a conversion element i.e. an energy conversion without storage (7).

$$i_{RDiffCell} = \frac{u_{RC}}{R_{DiffCell}} \quad (7)$$

The thermal part is reorganized to represent the effort and the flow variables (Fig. 6).

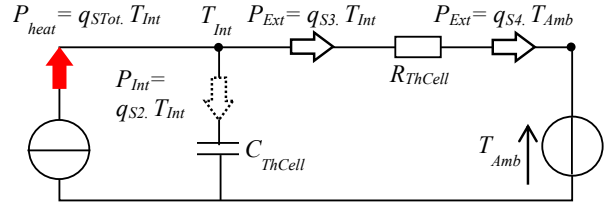


Fig. 6 Flow and effort variables for thermal model [17]

For thermal modelling, the effort variable is the temperature (K) and the flow variable is the entropy flow q_s (in W/K). The power P is achieved by multiplying those two variables (8):

$$P = q_s \cdot T \quad (8)$$

The entropy flows coming from R_{SCell} (9) and $R_{DiffCell}$ (10) are summed with a coupling pictogram (11):

$$q_{SRSCell} = \frac{R_{SCell} \cdot i_{Cell}^2}{T_{Int}} \quad (9)$$

$$q_{SRDiffCell} = \frac{R_{DiffCell} \cdot i_{RDiffCell}^2}{T_{Int}} \quad (10)$$

$$q_{STot} = q_{SRSCell} + q_{SRDiffCell} \quad (11)$$

In EMR, the thermal capacitance is an accumulation element, as there is a differential equation (12). This equation has been reorganized for EMR in [18]. Variables are the temperature, T (K), and the entropy flow, q_s (W/K) (13). The equation is described in an integral form (14).

$T_{IntInit}$ is the initial internal temperature of the cell.

$$\frac{dT_{Int}}{dt} = \frac{P_{Int}}{C_{ThCell}} \quad (12)$$

$$\Leftrightarrow \frac{dT_{Int}}{dt} = \frac{(q_{STotCell} - q_{S3}) \cdot T_{Int}}{C_{ThCell}} \quad (13)$$

$$\Leftrightarrow T_{Int} = T_{IntInit} \cdot e^{\frac{1}{C_{ThCell}} \int_0^t (q_{STotCell} - q_{S3}) dt} \quad (14)$$

The ambient air is considered as a source of temperature. The thermal resistance is a conversion element (15), (16).

$$q_{S3} = \frac{T_{Int} - T_{Amb}}{(R_{ThCell}) \cdot T_{Int}} \quad (15)$$

$$q_{S4} = \frac{T_{Int} - T_{Amb}}{(R_{ThCell}) \cdot T_{Amb}} \quad (16)$$

As R_{SCell} and $R_{DiffCell}$ are present in the thermal and electrical parts, they are represented as multi-physical (electro-thermal) converters.

All of the electrical parameters (OCV_{Cell} , R_{SCell} , $R_{DiffCell}$, $C_{DiffCell}$) are dependent on both the internal temperature and the SoC of the cell. The thermal parameters are constant, as they are related to geometry and mass of the cell.

C. Building the battery model

The battery of the studied EV is composed of 24 cells in series. For mass repartition purpose, the battery is divided into 3 modules (7/10/7 cells). They are placed at different locations (2 under the seats and one under the front hood). In a module, the cells are placed in line and separated by cooling holes (Fig. 7).

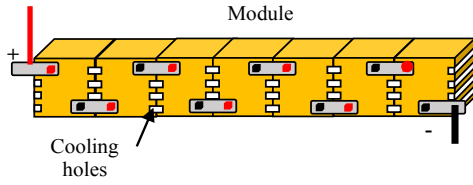


Fig. 7 Module 1 setup in the studied EV

The corresponding battery model is built with the two following assumptions:

- There is no parameters variation between the cells.
- The cooling holes make the thermal interactions between the cells negligible. As a consequence, the thermal part of the cell model is considered unchanged in this particular EV battery.

These strong assumptions will be validated by comparisons between simulation and experimental measurement in the vehicle (see section IV).

The connection resistance between cells has been estimated at $R_{Con}=505 \mu\Omega$ by measurements in the vehicle during driving tests. It is considered as a constant for simulation. A conversion pictogram (17) is added to the cell EMR (Fig 8).

$$u_{Cell} - R_{Con} \cdot i_{Cell} = u_{CellCon} \quad (17)$$

where $u_{CellCon}$ is the voltage for one cell with connections. The electrical model is deduced from the cell model (18). In EMR, it corresponds to an adaptation element i.e. power amplification:

$$\begin{cases} u_{CellCon} \cdot 7 = u_{Mod1} \\ i_{Cell} = i_{Mod1} \end{cases} \quad (18)$$

where u_{Mod1} and i_{Mod1} are the module voltage and current. Then a second adaptation element is added (see Fig. 8) to build up to the battery model (19).

$$\begin{cases} u_{Mod1} \cdot \frac{24}{7} = u_{Bat} \\ i_{Mod1} = i_{Bat} \end{cases} \quad (19)$$

where u_{Bat} and i_{Bat} are the battery voltage and current.

D. Integration of the battery model and the EV model

The EV used for the test is a Tazzari Zero [26]. This is a two-seat urban electric car. Its parameters can be found in

Table 1. A global efficiency map has been derived from measurements [1], including the electric drive efficiency (η_{Drive}). Equations (20)-(23) are organized in a causal way to be included in the global EMR (see Fig. 8).

$$\begin{aligned} \text{Electric Drive} \quad i_{Bat} &= \eta_{Drive}^k \frac{\Omega_{drive} \cdot T_{drive}}{u_{Bat}} \\ k &= 1 \text{ if traction mode} \\ k &= -1 \text{ if regenerative braking} \end{aligned} \quad (20)$$

$$\begin{aligned} \text{Transmission} \quad \begin{cases} T_{Drive} \cdot k_{Drive} \cdot \frac{1}{r_{Wheel}} = f_{Tract} \\ \Omega_{Drive} = \frac{1}{r_{Wheel}} \cdot k_{Drive} \cdot v \end{cases} \end{aligned} \quad (21)$$

$$\text{Chassis} \quad v = \frac{1}{M_{Tot}} \int_0^t f_{Tract} - f_{Res} dt \quad (22)$$

$$\text{Road} \quad f_{Res} = f_0 + \frac{1}{2} c_x S \varphi_{Air} v^2 \quad (23)$$

where Ω_{Drive} and T_{Drive} are the electric drive speed, and torque. Ω_{Wheel} and T_{Wheel} are the speed and torque at the wheel. f_{Tract} and f_{Res} are the traction and resistive forces. v_{Veh} is the velocity of the vehicle. Other parameters are defined in

Table 1.

The electric drive is a multi-physical (electro-mechanical) converter (20), the mechanical transmission is a mono-physical converter (21) and the chassis is an accumulation element (22). The road is a source of resistive forces (23). EMR allows us to determine the control structure by a mirror effect (24), (25).

The velocity control is achieved by the inversion of the chassis and the transmission in order to provide the right reference torque to the electric drive ($T_{DriveRef}$) in order to follow the velocity reference (v_{Ref}). The control pictograms are represented in blue in Fig. 8.

$$\begin{aligned} \text{Inv. Chassis} \quad f_{TractRef} &= f_{ResMes} + C(s) \cdot (v_{Ref} - v_{Mes}) \end{aligned} \quad (24)$$

$$\begin{aligned} \text{Inv. Transmission} \quad T_{DriveRef} &= \frac{r_{Wheel}}{k_{Drive}} \cdot f_{TractRef} \end{aligned} \quad (25)$$

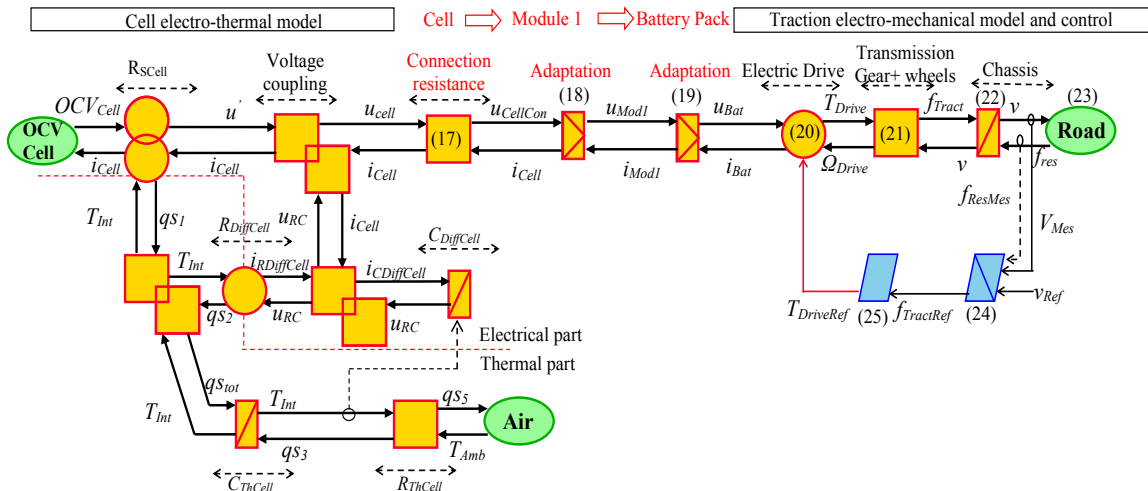


Fig. 8 EMR of the Tazzari Zero with control

III. CHARACTERIZATION OF ONE CELL

A. Electrical Characterization

The electrical parameters of the cell are dependent on temperature. Consequently, they are characterized every 15 °C. The characterization temperature range (-5 °C, 55 °C) is an acceptable range of temperature for EV batteries in temperate countries [27]. The characterization protocol is composed of 4 steps and repeated for all of the characterized temperatures.

1. Recharge @ 25 °C: in order to begin systematically with the same amount of stored energy, the initial charge is made after a minimal rest (i.e. $i_{Cell}=0A$) of 8h at 25°C. The recharge method is a constant-current-constant-voltage with a cut-off voltage of 4V. The cut-off current is 8A (C/20). This provides a reproducible reference SoC (100 %) at the end of this step.

2. Characterization temperature stabilisation: the cell is put at rest and the temperature is settled at the characterization temperature for at least 8h to equalize the cell internal temperature with the characterization temperature.

3. Pseudo OCV characterization: the discharge/ charge is achieved at low C-rate (C/10 = 16 A).

4. Pulse characterization: the impedance parameters of the electrical model are characterized at different SoC levels with current pulses (+/-1C). The SoC selected levels are 90 %, 70 %, 50 %, 30 % and 10 %.

With the pseudo-OCV characterization, the charge and discharge capacity can be extracted (26):

$$C_{AhCell} = \frac{1}{3600} \int_0^{t_{Ch/Dch}} |i_{Cell}| dt \quad (26)$$

C_{AhCell} is the cell capacity (A.h). $t_{Ch/Dch}$ is the total charge or discharge time to achieve the full charge or discharge (from 2.8 V to 4.0 V). The capacity C_{AhCell} versus temperature evolution is presented in Fig. 9. The capacity increases with the temperature as in [5]. Above 25 °C, the maximal measured capacity (192 A.h) is reached. This value is 20% higher than the rated one (160 A.h). It might correspond to the margin of the manufacturer to provide at least 160 A.h capacity during the whole lifespan of the cell [28].

$OCV_{Cell} = f(SoC)$ is also characterized during the pseudo-OCV characterization. Indeed, at low current the measured cell voltage u_{Cell} is near to the OCV_{Cell} . A small difference is noticeable for OCV_{Cell} during charge and discharge (Fig. 10). This phenomenon is due to the battery OCV hysteresis [29].

During the pulse characterization (Fig. 11), a double characterization pulse inspired from the HPPC method [30] is applied (Fig. 11). Although the chosen characterisation method is leading to uncertainties on parameters, it has benefits of simplicity, reproducibility and because the current rates used are close to the actual use of the cells in the EV. For the sake of simplification, the extracted parameters (27)-(29) are an average between charge and discharge characterization pulses. The parameters for calculation are defined in Fig. 11.

$$R_{SCell} = \frac{\Delta U_{Cell1s}}{\Delta i_{Cell}} \quad (27)$$

$$R_{DiffCell} = \left| \frac{\Delta U_{Cell1s} - \Delta U_{Celltr}}{\Delta i_{Cell}} \right| \quad (28)$$

$$C_{DiffCell} = \frac{\tau_{Diff}}{R_{DiffCell}} \quad (29)$$

$$\Delta U_{RC} = |\Delta U_{Celltr} - \Delta U_{Cell1s}| \quad (30)$$

Fig. 12 shows the evolution of the impedance parameters as a function of ambient temperature and SoC. For 0 % and 100 % SoC, the parameters are extrapolated. The series resistance R_{SCell} represents the equivalent effect of the terminals, the transports of ions in the electrolyte and the charge transfer mechanisms. When the temperature increases, the electrolyte viscosity decreases and the ion movement is easier [31].

Thus, R_{SCell} is decreasing with increasing temperature and it is independent of the SoC (see Fig. 12).

At low SoC, the positive electrode is nearly saturated with lithium. Thus, the insertion and diffusion of ions is more difficult, causing greater concentration gradient (increase of $R_{DiffCell}$). The diffusion capacitance $C_{DiffCell}$ increases with SoC and temperature.

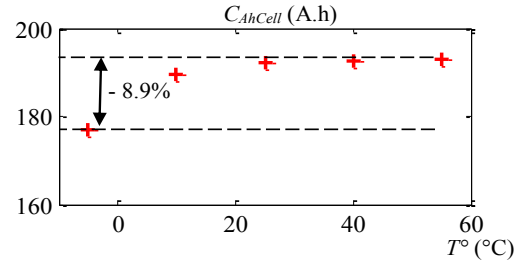


Fig. 9 Evolution of capacity with ambient temperature

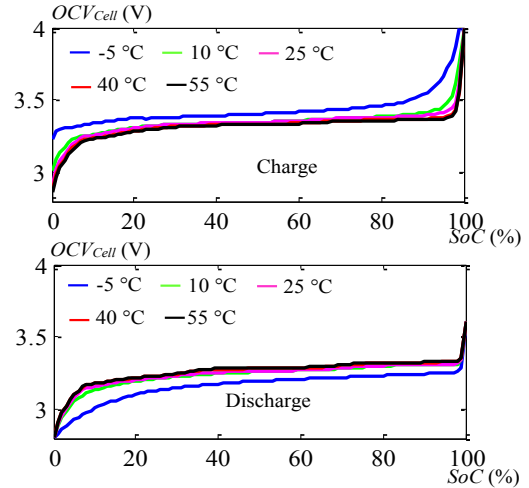


Fig. 10 OCV vs. SoC and temperature

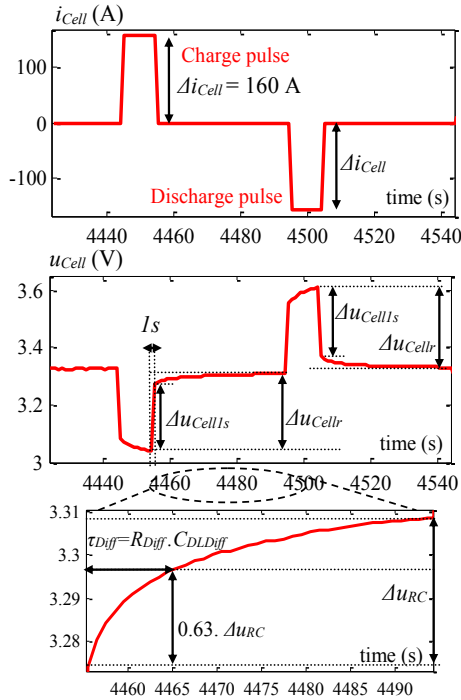


Fig. 11 Characterization pulses

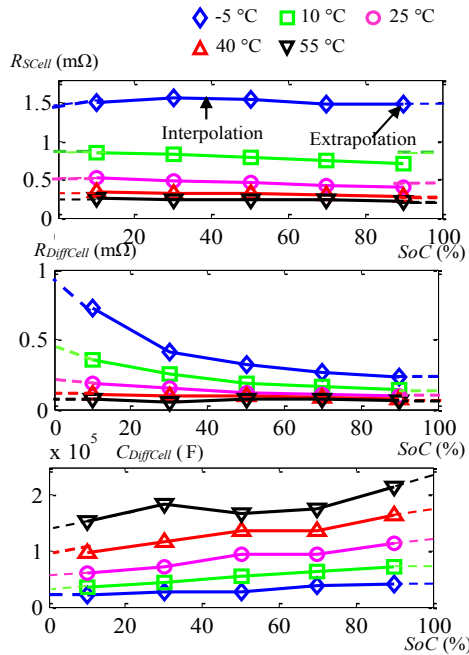


Fig. 12 Impedance parameters with SoC and temperature

B. Thermal characterization

The thermal parameters are characterized at 25 °C (Fig. 13). They are mainly related to the mass of the cell and the thermal exchange surface (independent from the ambient temperature).

The internal temperature of the tested cell is estimated at the terminals with thermocouples (closest accessible points to the averaged internal cell temperature [25]).

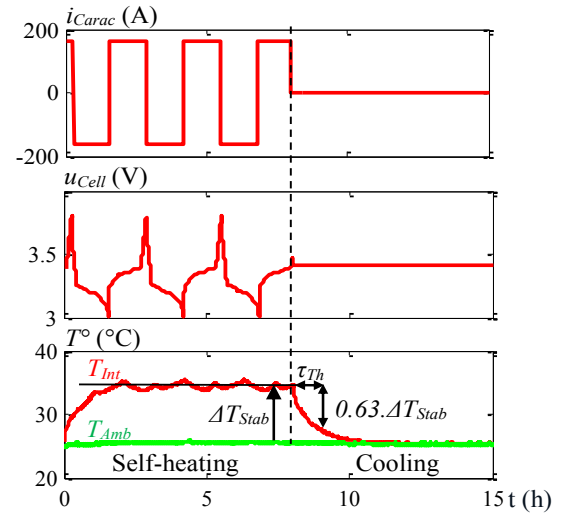


Fig. 13 Thermal characterization protocol

Indeed, terminals are linked to the core of the cell by metallic foils with high thermal conductivity. The ambient temperature of the air around the cell is recorded by a supplementary thermocouple. The cell is placed in a thermal chamber. The temperature is settled at 25 °C for 8h in order to equalize the cell internal temperature (T_{Int}) with the ambient temperature. Then the characterization process presented in Fig. 13 is applied.

At first, a characterization current (+/- 160 A) is applied until the temperature T_{Int} is stabilized (self-heating step) [25].

The stabilised temperature difference (ΔT_{Stab}) can be measured. This step is used to identify the value of R_{ThCell} .

$$R_{ThCell} = \frac{\Delta T_{stab}}{P_{Heat}} = 2.60 \text{ K} \cdot \text{W}^{-1} \quad (31)$$

Then the characterization current is turned off and the temperature T_{Int} is decreasing (cooling step). The extraction of the thermal time constant τ_{Th} is achieved (see Fig. 13). The thermal capacitance is extracted with (4):

$$C_{ThCell} = \frac{\tau_{Th}}{r_{ThCell}} = 2.43 \cdot 10^3 \text{ J} \cdot \text{K}^{-1} \quad (32)$$

IV. VALIDATION OF THE MODEL

A. Validation at the cell level (subsystem level in laboratory)

The tested EV has been instrumented with voltage sensors, current sensors and thermocouples. The cell current is recorded during a real driving cycle on a campus [32]. As the velocity is limited to 30 km/h on the campus, the current as a function of time is moderate (Fig. 14.a).

Additionally, in a laboratory, the real current cycle is applied to one cell with a high-power programmable supply (0-30 V -200/+200A) until the minimal cell voltage (i.e. 2.8 V) is reached (Fig. 14.b). The experimental cell voltage (u_{Cell}) and temperature (T_{Int}) are recorded. The test is performed for 4 ambient temperatures (-5 °C, 10 °C, 25 °C, 40 °C) in a thermal chamber.

The experimental results ($u_{CellExp}$, T_{IntExp}) are compared to the simulation outputs ($u_{CellSim}$, T_{IntSim}) for the same input, i.e. the current of the cycle.

Two models are considered:

- the classical model with the parameters characterized at 25°C (Param@25°C),
- The second model with the characterizations at different temperatures to update the electrical parameters.

Contrary to [33], no adaptive observer is used to adapt the value of parameters. For illustration purpose, the cell voltage evolution is presented as a function of time for an ambient temperature of -5 °C (Fig. 14.b). The red curve corresponds to the experimental data, the black one to the classical model and the blue one to the temperature-dependent model. Taking into account the impact of temperature on electrical parameters brings more accuracy for cell voltage dynamical and static behaviour at low temperature.

The mean absolute error on voltage is then quantified with (33) for different temperatures.

$$Error = \frac{1}{N_s} \sum_{i=1}^{N_s} |u_{CellExp} - u_{CellSim}| \quad (33)$$

where N_s is the number of samples during the test.

The model that includes temperature dependence leads to an average error on u_{Cell} (~1%) relative to $u_{CellNom}$ (3.3V) at any temperature (Fig. 14.b). The use of a, HPPC-type characterisation without correction leads to uncertainty in the impedance parameters. As a consequence, most of the average error occurs when the current peaks (thus voltage drops) are

high (see zoom in Fig. 14.b). When the current is near zero (from 2.54 h to 2.58 h), the experimental voltage of the cell and the voltage of the coupled electro-thermal model are the same. That means that the pseudo OCV is estimated with lower error than u_{Cell} by the model. On the contrary, using the parameters characterized at 25 °C induces a 124 mV (3.8% compared to the 3.3 V nominal voltage) error at -5 °C. The error is increasing when temperature is decreasing because of the decrease in the capacity and the increase of the series and diffusion resistances.

Fig. 14.c presents the evolution of cell temperature for different ambient temperatures.

The mean absolute error (34) is also presented:

$$Error = \frac{1}{N_s} \sum_{i=1}^{N_s} |T_{IntExp} - T_{IntSim}| \quad (34)$$

For low temperatures (up to 10 °C) the temperature effect on electrical parameters changes the accuracy of the temperature estimation (Fig. 14.c). The maximal error is 1.7 °C at -5°C. For temperatures higher than 25 °C, the effect of the temperature on the electrical parameters is lower.

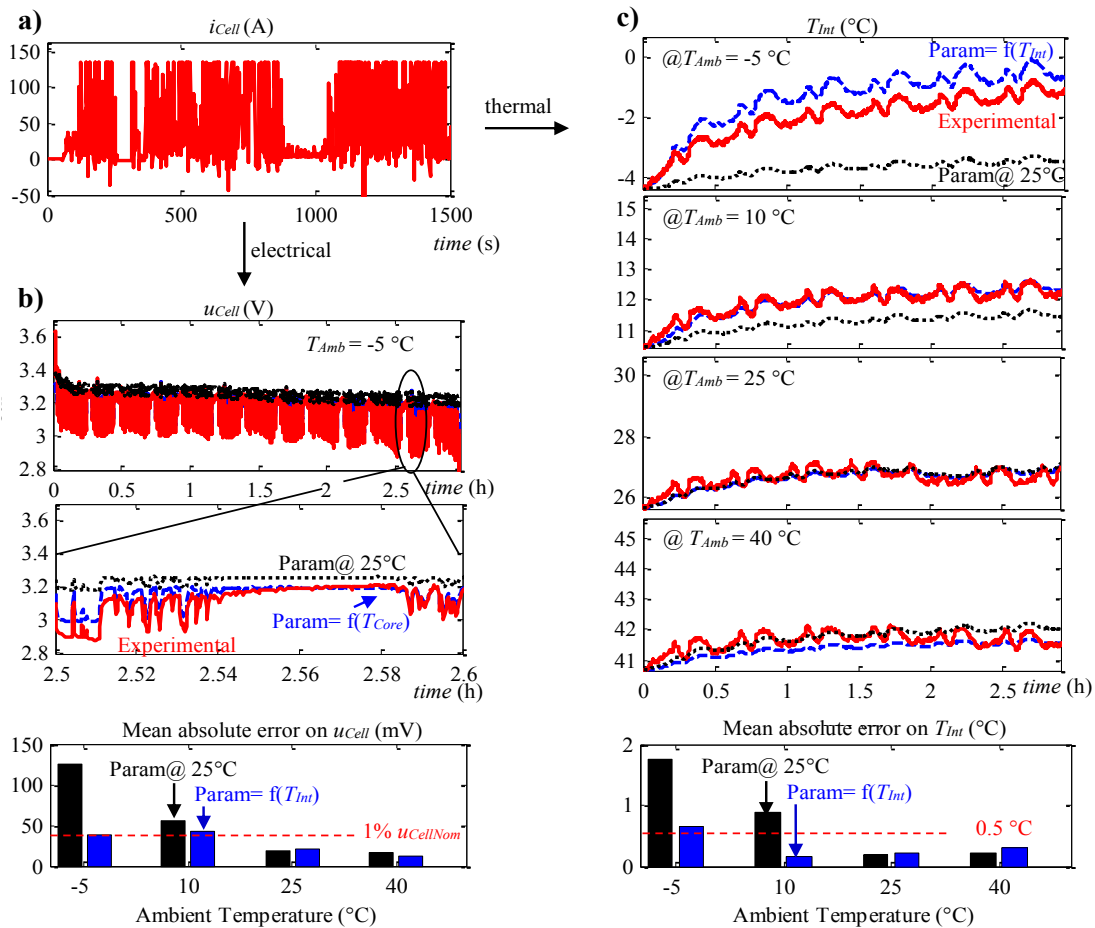


Fig. 14 Real EV current (a) used for electrical (b) and thermal (c) validation of cell model

B. Validation at the system level

This section validates the battery electro-thermal model at the system level (on-board tests on the real EV). The battery model and the traction models are thus coupled in dynamic interaction (see Fig. 8).

The tested EV is instrumented for the following measurements during driving:

- the battery current (i_{BatExp}),
- the ambient temperature around the battery (T_{AmbExp}) and the battery voltage (u_{BatExp}),
- the temperature on one terminal of one cell in the battery ($T_{TermExp}$).
- the vehicle velocity (used as a reference for the model).

The EV is driven for 6000s. A new velocity cycle is recorded (Fig. 15) outside the campus. This cycle is applied as a reference for the simulation (Fig. 8).

The experimental results and the proposed dynamically coupled EV model simulation results are compared for thermal (Fig. 16) and electrical (Fig. 17) behaviors. The measured temperature ($T_{TermExp}$) is influenced by the internal temperature of the cell. Indeed, the terminals are linked to the core of the cell by aluminium foils (high thermal conductivity). The connection temperature also influences $T_{TermExp}$. As the cell mass is much higher than the connection mass, the cell thermal dynamics are assumed to be slow compared to the connection one. As a consequence, the internal temperature (T_{IntEst}) is estimated by a low pass filter on the measured terminal temperature.

The comparison shows weak errors on the battery thermal and electrical behaviors. Of course, the chosen assumptions of the battery electro-thermal model depend on the pack architectures, the cells, the studied vehicle and the driving cycle. For the chosen vehicle, all cells are assumed identical and not thermally influenced by the surrounding cells. However, acceptable simulation results are obtained with averaged errors of about 1°C for internal temperature and 2 % on battery voltage. More accurate models should be studied in future work.

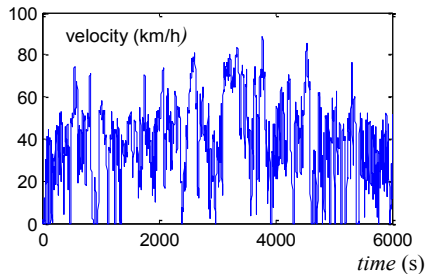


Fig. 15 Recorded velocity of the tested EV

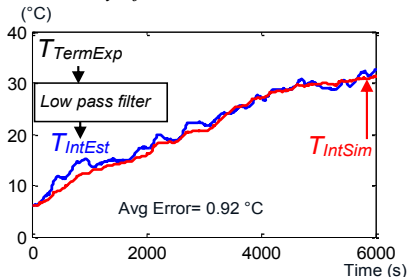


Fig. 16 Experimental and simulated battery temperature

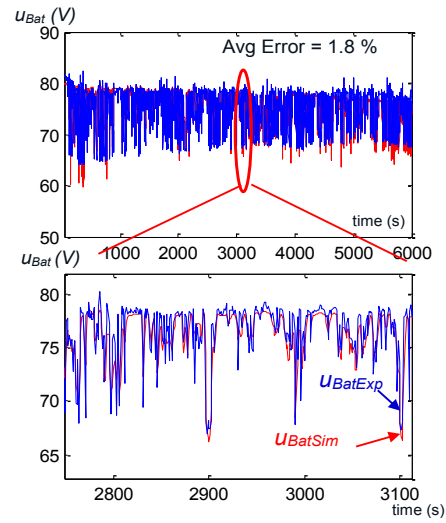


Fig. 17 Experimental and simulated battery voltage

V. APPLICATION OF THE ELECTRO-THERMAL-TRACTION DYNAMICAL COUPLED MODEL

The driving range of a vehicle is obtained by coupling the battery model with the traction model (simulation at the system level). Simulation is preferred to experiments in this section because it allows to exactly reproduce the same driving cycle, which is not possible when driving because of traffic conditions, driver variability, climatic conditions, etc. The battery model has been experimentally validated in the previous section and the traction model in [1]. The reference cycle is a velocity cycle (see Fig 8).

Thus, two battery models are studied:

- For the classical battery electrical model, the electrical parameters are fixed to their values at 25°C.
- For the electro-thermal coupled model, the electrical parameters are dependent on the battery internal temperature (T_{Int}).

The WLTC driving cycle (Fig. 18) is applied to the full EV model including its velocity control (see Fig. 8).

When the EV traction is coupled, the current is adapted from the battery voltage in order to achieve the same velocity cycle. The resistive parts of the model are influenced by cold temperatures (Fig. 12).

As a consequence, the current consumption is higher at low temperature for the proposed model (Fig. 19). The driving range is increased by 5.9 % between -5 °C and 45°C of ambient temperature (Fig. 20). The classic electrical battery model overestimates the driving range by 3.3% at -5 °C and underestimates it by 2.5% at 40°C.

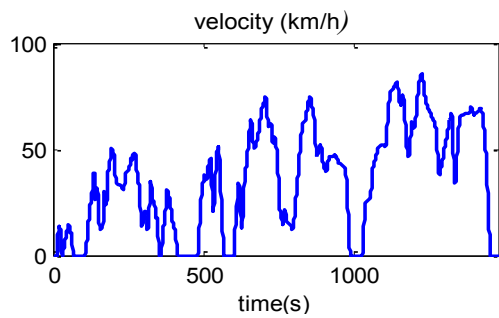


Fig. 18 WLTC driving cycle

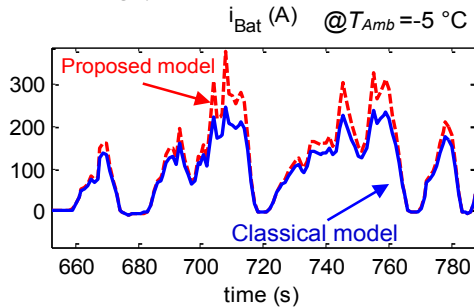
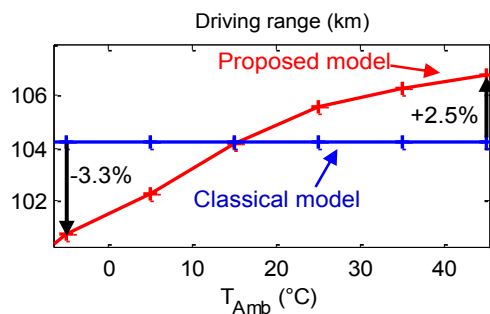
Fig. 19 Battery current at -5°C 

Fig. 20 Driving range as a function of ambient temperature

VI. CONCLUSION

The developed battery model aims to study the impact of ambient temperature on the driving range of an EV. In that objective, a battery model has been developed with a dynamical coupling between the thermal and electrical elements. A dynamic coupling of this battery model with the dynamic model of the traction subsystem has also been achieved. The electrical part of the battery model is fully dependent on the battery internal temperature and the SOC.

Characterization tests have been performed on one cell used in the studied EV. The battery parameters are thus obtained over a large temperature range (-5°C to 55°C). This range corresponds to EV use in temperate countries. The coupled electro-thermal model for one cell is validated at the component level in a thermal chamber with a programmable current supply. It is also compared with an electro-thermal model with fixed electrical parameters characterized at 25°C (though any other characterization temperature can be used). The electro-thermal dynamical coupling influences the cell behaviour at low temperature. Then, the battery electro-thermal model is validated at the system level by comparison of the full EV simulation and on-board measurements during driving.

Finally, a driving range study is realized using the electro-thermal model integrated in EV simulation. Neglecting the electro-thermal coupling of the battery model (using a pure electrical battery model) overestimates the driving range by 2.5% at -5°C ambient temperature and underestimates it by 2.5% at 40°C . These values depend on the EV and the chosen driving cycle but they indicate a relevant trend in the driving range.

This battery model could be also coupled to models of the heating system in winter or air conditioning in summer for more global energy consumption study. This model could be also used for study of the impact of battery preheating or any other thermal management [13] before driving. Future work could improve the accuracy of this model (e.g. more complex Thevenin models, thermal interactions between cells, cell parameters dispersion, variable contact resistance, efficiency map for machines, etc).

VII. BIBLIOGRAPHY

- [1] C. Dépature, W. Lhomme, A. Bouscayrol, P. Sicard, L. Boulon, "Efficiency map of the traction system of an electric vehicle from an on-road test drive", *IEEE Vehicle Power and Propulsion Conference*, Coimbra (Portugal), Oct. 2014.
- [2] X. Li, C. Liu, et J. Jia, « Ownership and Usage Analysis of Alternative Fuel Vehicles in the United States with the 2017 National Household Travel Survey Data », *Sustainability*, vol. 11, no 8, p. 1-16, 2019.
- [3] A. Cappelto et al., « Performance of wide temperature range electrolytes for Li-Ion capacitor pouch cells », *J. Power Sources*, vol. 359, p. 205-214, Aug. 2017.
- [4] J. Jaguemont, L. Boulon, et Y. Dubé, « A comprehensive review of lithium-ion batteries used in hybrid and electric vehicles at cold temperatures », *Appl. Energy*, vol. 164, p. 99-114, Feb. 2016.
- [5] J. P. Singer et K. P. Birke, « Kinetic study of low temperature capacity fading in Li-ion cells », *J. Energy Storage*, vol. 13, p. 129-136, Oct. 2017.
- [6] J. Jaguemont, L. Boulon, P. Venet, Y. Dube, et A. Sari, « Lithium-Ion Battery Aging Experiments at Subzero Temperatures and Model Development for Capacity Fade Estimation », *IEEE Transactions on Vehicular Technology*, vol. 65, no 6, p. 4328-4343, June 2016.
- [7] I. Baghdadi, O. Briat, J.-Y. Deléage, P. Gyan, et J.-M. Vinassa, « Lithium battery aging model based on Dakin's degradation approach », *J. Power Sources*, vol. 325, p. 273-285, Sept. 2016.
- [8] C. Forgez, D. Vinh Do, G. Friedrich, M. Morcrette, et C. Delacourt, « Thermal modeling of a cylindrical LiFePO₄/graphite lithium-ion battery », *J. Power Sources*, vol. 195, no 9, p. 2961-2968, May 2010.
- [9] X. Hu, S. Lin, S. Stanton and W. Lian, "A Foster Network Thermal Model for HEV/EV Battery Modeling," in *IEEE Transactions on Industry Applications*, vol. 47, no. 4, pp. 1692-1699, July-Aug. 2011.
- [10] J. Jaguemont, L. Boulon, et Y. Dubé, « Characterization and Modeling of a Hybrid-Electric-Vehicle Lithium-Ion Battery Pack at Low Temperatures », *IEEE Transactions on Vehicular Technology*, vol. 65, no 1, p. 1-14, Jan. 2016.
- [11] H. E. Perez, X. Hu, S. Dey and S. J. Moura, "Optimal Charging of Li-Ion Batteries With Coupled Electro-Thermal-Aging Dynamics," in *IEEE Transactions on Vehicular Technology*, vol. 66, no. 9, pp. 7761-7770, Sept. 2017.
- [12] W. Mohammed, E. Kamal, A. Aitouche and A. A. Sobaih, "Development Of Electro-Thermal Model of Lithium-Ion Battery for Plug-In Hybrid Electric Vehicles," 2018 7th International Conference on Systems and Control (ICSC), Valencia, 2018, pp. 201-206.
- [13] J. Jaguemont, L. Boulon, Y. Dubé and F. Martel, "Thermal Management of a Hybrid Electric Vehicle in Cold Weather," in *IEEE Transactions on Energy Conversion*, vol. 31, no. 3, pp. 1110-1120, Sept. 2016.
- [14] Y. Cao, R. C. Kroeze, P. T. Krein, « Multi-timescale Parametric Electrical Battery Model for Use in Dynamic Electric Vehicle Simulations », *IEEE Transactions on Transportation Electrification*, vol. 2, no 4, p. 432-442, Dec. 2016.
- [15] A. Bouscayrol, J. P. Hautier, B. Lemaire-Semail, "Graphic Formalisms for the Control of Multi-Physical Energetic Systems", *Systemic Design Methodologies for Electrical Energy*, tome 1, Analysis, Synthesis and Management, Chapter 3, ISTE Wiley editions, October 2012, ISBN: 9781848213883.

- [16] G. Rizzoni, L. Guzzella, B.M. Baumann, "Unified modeling of hybrid electric vehicle drivetrains", *IEEE/ASME Transactions on Mechatronics*, Vol.4, no. 3, pp. 246 – 257, September 1999.
- [17] R. German, A. Desrevelaux, A. Bouscayrol, "Single Cell Electro-Thermal Model for Simulation of an Electric Vehicle," 2018 IEEE Vehicle Power and Propulsion Conference (VPPC), Chicago, IL, 2018, pp. 1-5.
- [18] L. Horrein, A. Bouscayrol, W. Lhomme, et C. Dépature, « Impact of Heating System on the Range of an Electric Vehicle », *IEEE Transactions on Vehicular Technology*, vol. 66, no 6, p. 4668-4677, June 2017.
- [19] T. Yuksel and J. J. Michalek, "Effects of regional temperature on electric vehicle efficiency, range, and emissions in the united states," *Environmental Science and Technology*, vol. 49, no. 6, p. 3974–3980, 2015.
- [20] K. Kambly, T. H Bradley, « Geographical and temporal differences in electric vehicle range due to cabin conditioning energy consumption", *Journal of Power Sources*, vol. 275, p. 468-475, Feb. 2015.
- [21] S. Bellocchi, G. Leo Guizzi, M. Manno, M. Salvatori, A. Zaccagnini, "Reversible heat pump HVAC system with regenerative heat exchanger for electric vehicles: Analysis of its impact on driving range," *Applied Thermal Engineering*, vol. 129, pp. 290–305, Jan. 2018.
- [22] S. Gantenbein, M. Weiss, E. Ivers-Tiffée, « Impedance based time-domain modeling of lithium-ion batteries: Part I », *Journal of Power Sources*, vol. 379, p. 317– 327, Mar. 2018.
- [23] N. Omar, P. Van den Bossche, T. Coosemans, J. Van Mierlo, "Peukert Revisited—Critical Appraisal and Need for Modification for Lithium-Ion Batteries", *Energies* 2013, 6(11), 5625-5641.
- [24] E. Riviere, A. Sari, P. Venet, F. Meniere, Y. Bultel, "Innovative Incremental Capacity Analysis Implementation for C / LiFePO4 Cell State-of-Health Estimation in Electrical Vehicles", *Journal Batteries*, vol. 5 (2), no. 37, April 1, 2019.
- [25] P. Kreczanik, P. Venet, A. Hijazi, et G. Clerc, « Study of Supercapacitor Aging and Lifetime Estimation According to Voltage, Temperature, and RMS Current », *IEEE Trans. Ind. Electron.*, vol. 61, no 9, p. 4895-4902, Sept. 2014.
- [26] Tazzari Group, « Tazzari Zero use and maintenance manual », 2009.
- [27] J. Lindgren et P. D. Lund, « Effect of extreme temperatures on battery charging and performance of electric vehicles », *Journal of Power Sources*, vol. 328, p. 37–45, Oct. 2016.
- [28] E. Redondo-Iglesias, P. Venet, et S. Pelissier, « Global Model for Self-Discharge and Capacity Fade in Lithium-Ion Batteries Based on the Generalized Eyring Relationship », *IEEE Transactions on Vehicular Technology*, vol. 67, no 1, p. 104–113, Jan. 2018.
- [29] Y. Wang, R. Pan, C. Liu, Z. Chen, et Q. Ling, « Power capability evaluation for lithium iron phosphate batteries based on multi-parameter constraints estimation », *J. Power Sources*, vol. 374, p. 12–23, Jan. 2018.
- [30] T. T. Lou, W. G. Zhang, H. Y. Guo, et J. S. Wang, « The Internal Resistance Characteristics of Lithium-Ion Battery Based on HPPC Method », *Advanced Materials Research*, 2012.
- [31] A. Berrueta, A. Urtaun, A. Ursúa, et P. Sanchis, « A comprehensive model for lithium-ion batteries: From the physical principles to an electrical model », *Energy*, vol. 144, p. 286–300, Feb. 2018.
- [32] A. Castaigns, W. Lhomme, R. Trigui, et A. Bouscayrol, « Practical control schemes of a battery/supercapacitor system for electric vehicle », *IET Electr. Syst. Transp.*, vol. 6, no 1, p. 20–26, 2016.
- [33] X. Lin et al., « Online Parameterization of Lumped Thermal Dynamics in Cylindrical Lithium Ion Batteries for Core Temperature Estimation and Health Monitoring », *Control Syst. Technol. IEEE Trans. On*, vol. 21, no 5, p. 1745–1755, Sept. 2013.



Ronan German was born in Roanne, France, in 1986. He received the master degree in electrical engineering at national institute of applied sciences of Lyon, France in 2009. From 2010 to 2013 he was a Ph.D. student from Lyon1 university under a joint supervision with Bordeaux I University. From 2013 to 2015 he made two years as an assistant professor at the University of Lyon. Since September 2015 he became an associate professor at the university of Lille in the Laboratory of Electrical Engineering and Power electronics (L2EP). His current research interests include management of energy storage systems in the context of electric vehicles as a function of various parameters.



Seïma Shili was born in Carthage, Tunisia, in 1987. She received the engineering degree in instrumentation and industrial maintenance from the National Institute of Applied Science and Technology, Tunis, Tunisia, in 2012, and the Ph.D. degree in electrical, engineering from University Claude Bernard Lyon 1, Lyon, France, in July 2016. Her current research interests include characterizations, fault diagnostics, reliability and ageing of energy storage systems such as film capacitors, supercapacitors and batteries, and also development of balancing, monitoring and management systems for energy storage systems.



Anatole Desrevelaux received the MS degree in electric engineering in 2016 from the University of Lille, France. Since 2016, he is currently pursuing the PhD degree in electrical engineering from the University of Lille, France. His work concerns the study of the energy consumption of an Electric Vehicle. His research interests concern the sustainable development of campus, the modeling and the control of Electric Vehicle. Anatole Desrevelaux is currently member of the French MEGEVH network.



Ali Sari is full professor at the University of Lyon, University Claude Bernard Lyon 1. He received the M.S. degrees in electrical engineering in 2006 and Ph.D. degrees, for his work on "Design of a mobile generator set with a Stirling engine and linear alternator", from the University of Franche-Comté in Belfort, France, in 2009. Since 2015, he is the head of electrical engineering and industrial informatics department of IUT Lyon 1. In Laboratory Ampère, his current research topics concerns ageing, reliability, diagnosis, maintainability and sustainability of energy storage systems (batteries, supercapacitors, capacitors). His research areas relate also development of balancing, monitoring and management systems for energy storage systems.




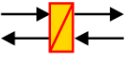







Pascal Venet received the Ph.D. degree in electrical engineering in 1993 from the Lyon 1 University, France. After postdoctoral positions, he joined the Lyon 1 University as Assistant Professor from 1995 to 2009. Since 2009, he has been Professor of Electrical Engineering at the Lyon 1 University. He has developed his research activity in an Electrical Engineering Laboratory (AMPERE). He is leader of the research team "Safe Systems and Energies" of the laboratory.

His current research interests include characterization, modeling, fault diagnostics, reliability and ageing of energy storage systems such as batteries, supercapacitors and capacitors. He also studies on BMS (Battery Management system) and therefore balancing of cells, determination of state of charge and state of health of battery.



Alain Bouscayrol received a Ph.D. degree in Electrical Engineering from the Institut National Polytechnique de Toulouse, France, in 1995. From 1996 to 2005, he was Associate Professor at University Lille1, France, where he has been a Professor since 2005. Since 2004, he has managed the national network on Energy Management of Hybrid Electric Vehicles France. He has initiated the Energetic Macroscopic Representation (EMR) in 2000 for the description and the control of energetic systems. His research interests at the L2EP include graphical descriptions for control of electric drives, wind energy conversion systems, railway traction systems, hybrid electric vehicles and hardware-in-the-loop simulation.

Appendix A: EMR Pictograms

	Source element (energy source)		Accumulation element (energy storage)		Indirect inversion (closed-loop control)
	Mono-physical conversion element		Mono-physical coupling element (energy distribution)		Direct inversion (open-loop control)
	Multi-physical conversion element		Multi-physical coupling element (energy distribution)		Coupling inversion (energy criteria)